Neurobiology of Disease 134 (2020) 104640

Contents lists available at ScienceDirect

Neurobiology of Disease

journal homepage: www.elsevier.com/locate/ynbdi

Functional screening of GATOR1 complex variants reveals a role for mTORC1 deregulation in FCD and focal epilepsy

Ruby E. Dawson[a,c], Alvaro F. Nieto Guil[b,c], Louise J. Robertson[b,c], Sandra G. Piltz[b,c], James N. Hughes[a,c], Paul Q. Thomas[b,c,d,*]

[a] School of Biological Sciences, University of Adelaide, Adelaide, SA 5005, Australia
[b] School of Medicine, University of Adelaide, Adelaide, SA 5005, Australia
[c] Robinson Research Institute, University of Adelaide, Adelaide, SA 5005, Australia
[d] Precision Medicine Theme, South Australia Health and Medical Research Institute, Adelaide, SA 5000, Australia

ARTICLE INFO

Keywords:
Neurodevelopment
Epilepsy
Focal cortical dysplasia
Molecular genetics
Functional testing
Developmental genetics
CRISPR/CAS9
Disease model
Mouse model
mTOR

ABSTRACT

Mutations in the GAP activity toward RAGs 1 (GATOR1) complex genes (*DEPDC5, NPRL2 and NPRL3)* have been associated with focal epilepsy and focal cortical dysplasia (FCD). GATOR1 functions as an inhibitor of the mTORC1 signalling pathway, indicating that the downstream effects of mTORC1 deregulation underpin the disease. However, the vast majority of putative disease-causing variants have not been functionally assessed for mTORC1 repression activity. Here, we develop a novel *in vitro* functional assay that enables rapid assessment of GATOR1-gene variants. Surprisingly, of the 17 variants tested, we show that only six showed significantly impaired mTORC1 inhibition. To further investigate variant function *in vivo*, we generated a conditional *Depdc5* mouse which modelled a 'second-hit' mechanism of disease. Generation of *Depdc5* null 'clones' in the embryonic brain resulted in mTORC1 hyperactivity and modelled epilepsy and FCD symptoms including large dysmorphic neurons, defective migration and lower seizure thresholds. Using this model, we validated *DEPDC5* variant F164del to be loss-of-function. We also show that Q542P is not functionally compromised *in vivo,* consistent with our *in vitro* findings. Overall, our data show that mTORC1 deregulation is the central pathological mechanism for GATOR1 variants and also indicates that a significant proportion of putative disease variants are pathologically inert, highlighting the importance of GATOR1 variant functional assessment.

1. Introduction

Focal epilepsy is a disease characterised by recurring seizures that occur in a localized region of the brain and can be caused by a range of environmental and genetic factors (Boillot and Baulac, 2016; Guo et al., 2013; Thomas and Berkovic, 2014). Recently, genes encoding the subunits comprising the GATOR1 complex, *NPRL2, NPRL3* and *DEPDC5*, were shown to be mutated in families with focal epilepsy (Baldassari et al., 2018; Dibbens et al., 2013; Ricos et al., 2016). In these patients, seizures occur at variable foci – indeed, affected individuals who carry the same germline mutation can have seizures originating from different cortical regions (Baldassari et al., 2018; Dibbens et al., 2013; Ricos et al., 2016). The severity of the disease symptoms also varies greatly, with cases of associated autism, cognitive delays and reports of Sudden Unexpected Death related to Epilepsy (SUDEP) (Bagnall et al., 2017; Nascimento et al., 2015; Weckhuysen et al., 2016). Some patients have focal cortical dysplasia (FCD) (type II), which involves defects in cortical lamination and the presence of large, dysmorphic neurons (Cen et al., 2017; Kabat and Król, 2012; Scerri et al., 2015; Weckhuysen et al., 2016).

Although GATOR1 mutations display autosomal dominant inheritance, there is also incomplete penetrance (Dibbens et al., 2013; Ricos et al., 2016). A somatic 'second-hit' mutation mechanism for GATOR1 epilepsies may underpin these diseases (D'Gama et al., 2017; Hu et al., 2018; Ribierre et al., 2018). It has been proposed that a second somatic mutation occurs in a neural progenitor cell of germline heterozygous patients, thereby generating a population of compound heterozygous cells that lacks GATOR1 function, from which seizures may arise. This is supported by two recent cases of *DEPDC5* epilepsy, in which somatic mutations have been identified in brain tissue isolated

* Corresponding author at: School of Medicine, University of Adelaide, Adelaide, SA 5005, Australia
E-mail addresses: ruby.dawson@adelaide.edu.au (R.E. Dawson), alvaro.nietoguil@adelaide.edu.au (A.F. Nieto Guil), louise.robertson@adelaide.edu.au (L.J. Robertson), sandra.piltz@adelaide.edu.au (S.G. Piltz), hugh0285@flinders.edu.au (J.N. Hughes), paul.thomas@adelaide.edu.au (P.Q. Thomas).

https://doi.org/10.1016/j.nbd.2019.104640
Received 6 May 2019; Received in revised form 7 October 2019; Accepted 13 October 2019
Available online 19 October 2019
0969-9961/ © 2019 Elsevier Inc. This is an open access article under the CC BY-NC-ND license (http://creativecommons.org/licenses/BY-NC-ND/4.0/).

from patients with germline heterozygous mutations (Baulac et al., 2015; Ribierre et al., 2018).

Previous *in vitro* studies have shown that GATOR1 functions to negatively regulate signalling of the mechanistic target of rapamycin complex 1 (mTORC1) pathway, with knockdown cell lines being insensitive to amino acid starvation, (Bar-Peled et al., 2013; Iffland et al., 2018). More recently, rodent models with global and focal *Depdc5* loss-of-function have also shown the importance of *Depdc5* in regulating mTORC1 *in vivo* (Hu et al., 2018; Hughes et al., 2017; Ribierre et al., 2018; Yuskaitis et al., 2017). The mTORC1 pathway is involved in regulating many important cellular processes such as cell growth, protein synthesis and autophagy, and its deregulation has been linked with diseases including cancer and epilepsy, through the mutation of other repressors of the pathway (D'Gama et al., 2017; Lipton and Sahin, 2014; Meng et al., 2013). Indeed, germline and somatic mutations have been found in other mTORC1 pathway genes such as *TSC1/2, AKT, PIK3CA* and *mTOR* itself, in cases of hemimegaloencephaly and FCD-related epilepsy (D'Gama et al., 2017; Møller et al., 2016; Park et al., 2018). As an inhibitor of mTORC1, mutations in GATOR1 are predicted to cause epilepsy through mTORC1 hyperactivity, although the mechanism by which mTORC1 hyperactivity causes epilepsy and associated pathologies is not known (Baulac, 2016).

Since their implication in epilepsy, a large number of GATOR1 gene variants have been identified (Baldassari et al., 2018). However, due to the complex mechanism of the disease, the causative status of many GATOR1 variants is unclear, confounding definitive diagnosis, genetic counselling, treatment strategies and prediction of disease outcomes. This is especially true for in-frame or missense mutations where the functional impact is often difficult to predict. Although bioinformatic and *in silico* predictions have provided clues for the functional outcome of these variants, the vast majority of GATOR1 mutations have not been functionally assessed (Baldassari et al., 2018; Ricos et al., 2016; van Kranenburg et al., 2015).

Here, we describe a novel *in vitro* functional assay to assess the impact of 17 putative pathogenic GATOR1 variants on regulation of the mTORC1 pathway. We also describe a unique conditional 'second-hit' *Depdc5* mouse model and use this system to perform further functional assessment of selected *DEPDC5* variants *in vivo*. We show that a subset of GATOR1 variants are functionally compromised, indicating that mTORC1 deregulation is central to the pathological mechanism underpinning GATOR1-related focal epilepsy. Remarkably, we also show that vast majority of GATOR1 missense variants are not functionally compromised, underlining the importance of functional assessment in ascribing pathogenic status.

2. Results

2.1. Generation of GATOR1 gene null cell lines

We initially generated HEK293T cell lines lacking functional *NPRL2*, *NPRL3* or *DEPDC5* using a CRISPR/CAS9 exon deletion frameshift strategy (Supplemental Fig. 1A-C). To assess the impact of GATOR1 loss-of-function on mTORC1 signalling, null cells were cultured in the absence of serum for 1 h. mTORC1 activity was then assessed *via* phosphorylation of S6 protein at Ser240/244 (p-S6), a well-validated downstream marker of mTORC1 activity (Bar-Peled et al., 2013; Hughes et al., 2017; Ribierre et al., 2018). As expected, mTORC1 activity was reduced in starved control cells compared to complete media (Figs. 1A, 2A, 3A). However, consistent with previous reports (Bar-Peled et al., 2013), null cells were unable to downregulate mTORC1 in starvation conditions, as indicated by the persistence of high p-S6 levels, comparable to those observed in complete media. Addition of the mTORC1 inhibitor rapamycin decreased mTORC1 activity in null cells (Figs. 1A, 2A, 3A). Identical results were obtained using independent GATOR1 null cell lines generated with different gRNAs (Supplemental Fig. 2A) confirming that the starvation insensitivity phenotype is due to mutation of *NPRL2*, *NPRL3* or *DEPDC5*.

2.2. Identification of functional mutants in GATOR1 complex genes

To assess the functional impact of reported pathogenic GATOR1 variants, we sought to develop a quantitative mTORC1 rescue assay. As a positive control, null cells were transiently transfected with a rescue expression construct encoding the corresponding WT GATOR1 gene and a GFP reporter. After 1-hour serum starvation, cells were stained for p-S6. In each null cell line, p-S6 was markedly reduced by expression of the rescue construct but not by GFP alone (Supplemental Figs. 3–5). To enable higher-throughput quantitative analysis, flow cytometry was performed on the transfected null cells in complete media and starvation conditions (Figs. 1C-D, 2C-D, 3C-D). In all GATOR1 null cell lines, expression of the rescue construct significantly increased in the proportion of cells with low p-S6 expression compared with GFP-only control cells ($P \leq 0.0001$, two-way ANOVA) (Figs. 1J, 2J and 3K).

Next, we used this rescue assay to assess the function of putative disease-causing variants in *NPRL2* (5), *NPRL3* (5) and *DEPDC5* (7) (Figs. 1B, 2B, 3B, Supplemental Fig. 6A, Table 1). The *NPRL2* missense variant L105P failed to rescue mTORC1 hyperactivity indicating complete loss-of-function (Fig. 1F, J). Steady-state expression of this variant was comparable to WT NPRL2, indicating that loss-of-function was not due to reduced protein levels (Fig. 1K). The two remaining *NPRL2* missense variants, T110S and D214H, had comparable function to WT NPRL2 (Fig. 1G-H, J). Interestingly, variant R34*, although truncated at 34 amino acids, was also not significantly different to WT NPRL2 with ~22% of cells inhibiting mTORC1 in starved conditions above background levels (Fig. 1E, J). This is likely due to a second isoform produced from an internal initiation codon, which was detected by western blot analysis and may be functional at higher than endogenous levels of expression (Fig. 1K) (Hesson et al., 2007). Surprisingly, nonsense mutant R295* was also able to rescue the mTORC1 hyperactivity, despite a drastic reduction in protein size (Fig. 1I-K).

Both *NPRL3* missense mutations (R92Q, E249K) were functionally intact (Fig. 2E-F, J). In contrast, the remaining three variants, all of which were premature termination mutations (S279F fs*52, W319P fs*13, S460P fs*20), had significantly reduced activity compared to NPRL3 WT (Fig. 2G-I, J). It should be noted that variant S460P fs*20 retained some function as seen by the slight but significant increase in cells with low mTORC1 in starved conditions, when compared with complete media conditions ($P \leq 0.05$, unpaired *t*-test) (Fig. 2J). Western blot analysis of mutant proteins revealed similar expression levels to WT and the expected size reduction of the truncation mutants (Fig. 2K).

From the seven *DEPDC5* variants tested, one indel mutation (F164del) and one nonsense mutation (D1556*) had significantly reduced function (Fig. 3E, J, K). The former is an in-frame phenylalanine deletion which produces near full-length protein (Fig. 3L). Notably, we did see a slight, but not significant ($p = .068$, unpaired t-test) increase in F164del-expressing cells which repressed mTORC1 in starved conditions when compared to complete media, suggesting that some function may be retained in this mutant (Fig. 3E,K). Flow cytometry indicated that this mutant has increased activity at high levels of expression (Fig. 3E). D1556* is a *de novo* nonsense mutation close to the stop codon, only truncating 39 amino acids of the full length protein. The loss-of-function of this variant is potentially due to protein instability, as seen by low protein expression on western blot (Fig. 3I, K-L). The four other *DEPDC5* variants, all of which encoded missense mutations, did not have significantly altered function (Fig. 3F–H, K, Supplemental Fig. 6A–D).

These results were replicated and validated with independent *NPRL2*, *NPRL3* and *DEPDC5* null cell lines, showing there were no confounding effects from potential off-target mutations (Supplemental Fig. 2B–D). Overall, the majority of patient variants tested in this assay did not exhibit significant loss-of-function. Indeed, of the 17 variants

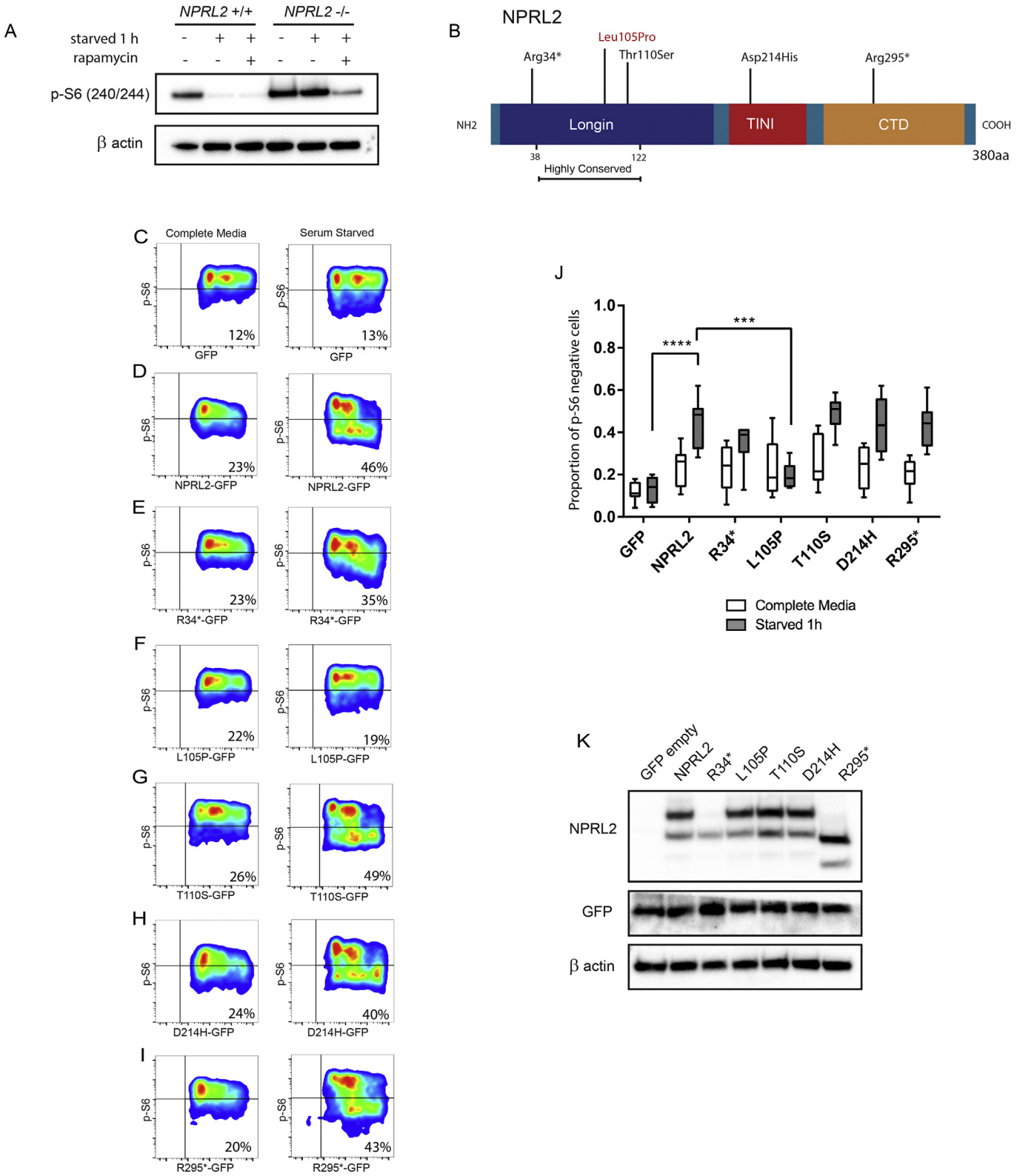

Fig. 1. Functional testing of *NPRL2* variants. (A) mTORC1 activity is unable to be downregulated in serum starved *NPRL2* null cells compared to empty vector controls, as shown by persistent p-S6 staining on western blot. Addition of rapamycin rescues the null cell ability to repress p-S6. **(B)** Schematic representation of *NPRL2* with patient variants. The variant in red was shown to be a loss-of-function mutant. **(C–I)** Representative plots of flow cytometry analysis performed on null cells transfected with variant constructs containing GFP in complete media and starved conditions, and staining for p-S6. Mean percentage of cells in bottom right quadrant is indicated inside plots. **(J)** Box and whisker plot of quantification of transfected cells with low mTORC1 activity determined by flow cytometry analysis, indicating variant functional ability to repress mTORC1 in starved conditions (**** = $p < .0001$, *** = $p < .001$, Two-way ANOVA with Dunnett's multiple comparisons tests, $n = 5–7$). **(K)** Western blot showing expression of *NPRL2* variants and GFP marker in lysates of transfected *NPRL2* null cells. (For interpretation of the references to colour in this figure legend, the reader is referred to the web version of this article.)

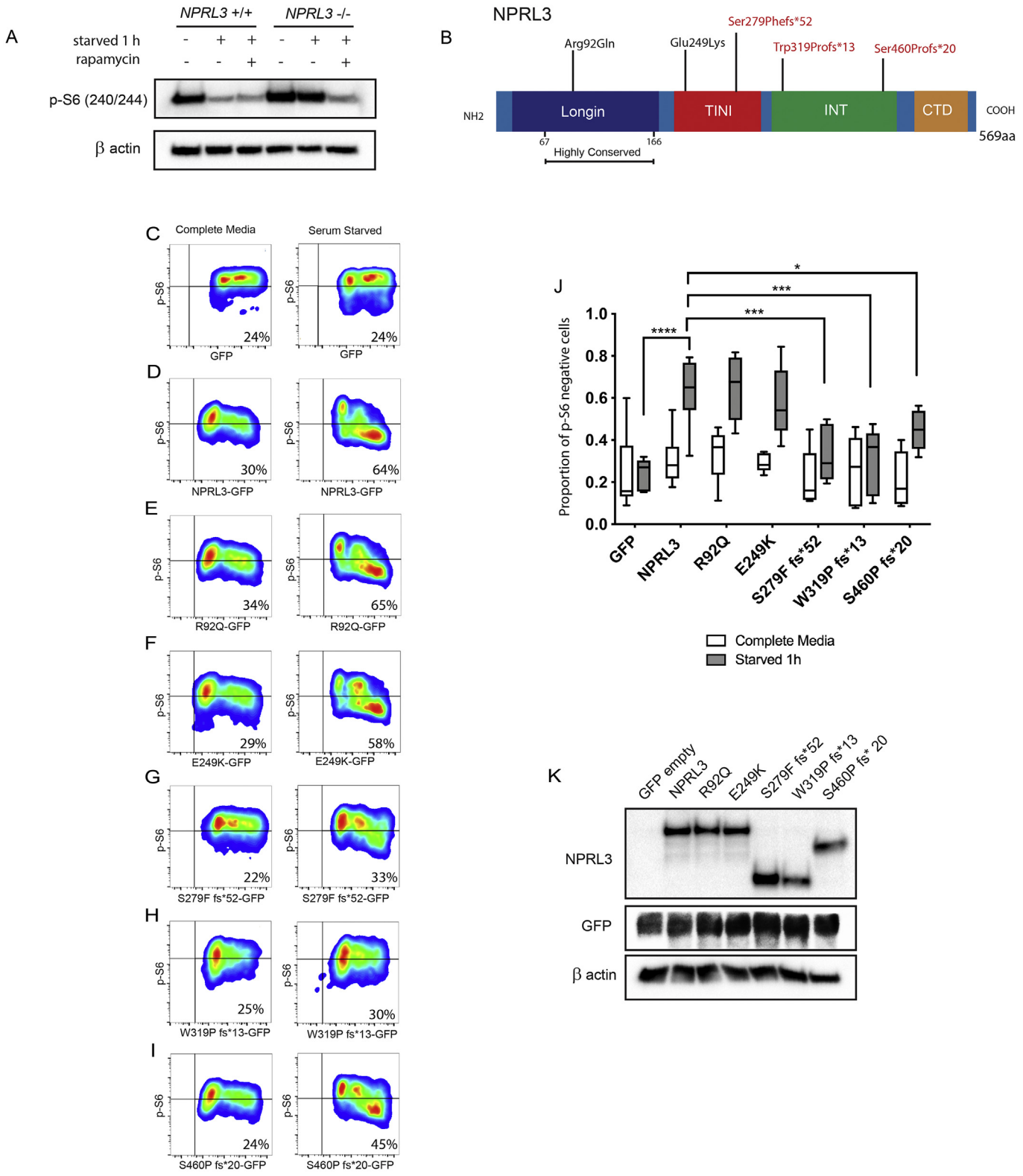

Fig. 2. Functional testing of *NPRL3* variants. (A) mTORC1 activity is unable to be downregulated in serum starved *NPRL3* null cells compared to empty vector controls, as shown by persistent p-S6 staining on western blot. Addition of rapamycin rescues the null cell ability to repress p-S6. **(B)** Schematic representation of *NPRL3* with patient variants. Variants in red were shown to be loss-of-function mutants. **(C–I)** Representative plots of flow cytometry analysis performed on null cells transfected with variant constructs containing GFP in complete media and starved conditions, and staining for p-S6. Mean percentage of cells in bottom right quadrant is indicated inside plots. **(J)** Box and whisker plot of quantification of transfected cells with low mTORC1 activity determined by flow cytometry analysis, indicating variant functional ability to repress mTORC1 in starved conditions (**** = $p < .0001$, *** = $p < .001$, * = $p < .05$, Two-way ANOVA with Dunnett's multiple comparisons tests, $n = 5–9$). **(K)** Western blot showing expression of *NPRL3* variants and GFP marker in lysates of transfected *NPRL3* null cells. (For interpretation of the references to colour in this figure legend, the reader is referred to the web version of this article.)

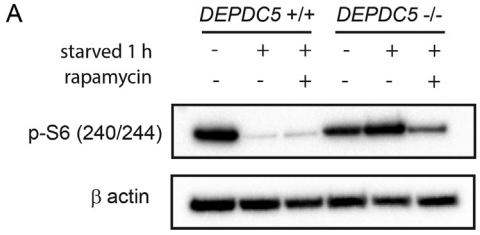

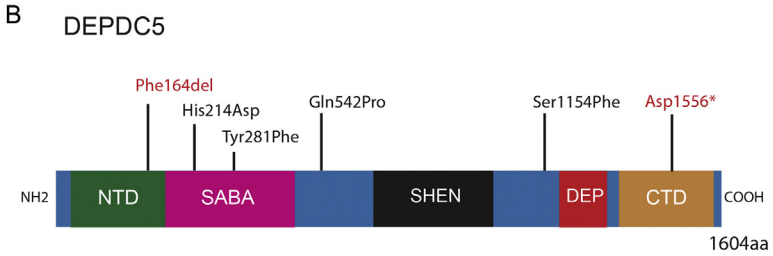

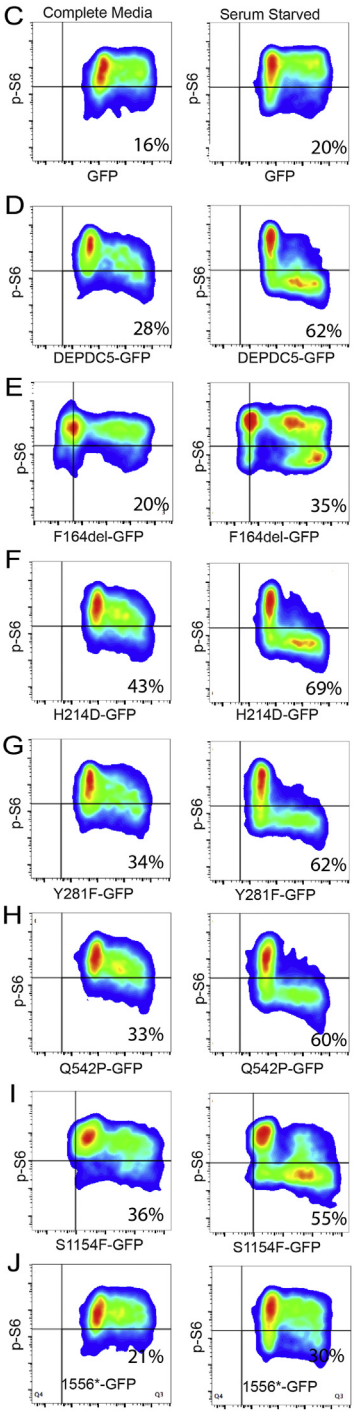

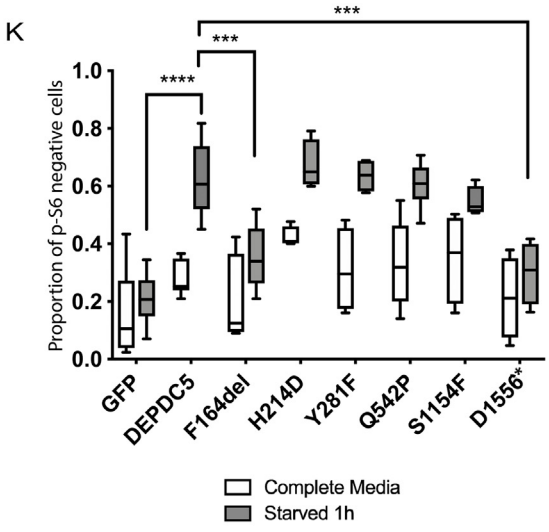

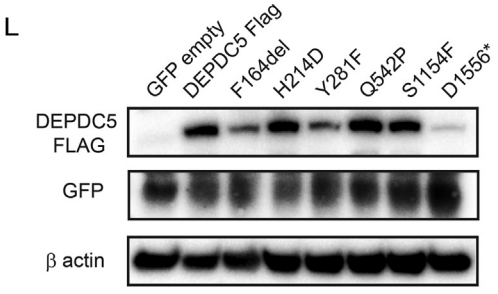

(caption on next page)

Fig. 3. Functional testing of*DEPDC5* variants. (A) mTORC1 activity is unable to be downregulated in serum starved *DEPDC5* null cells compared to empty vector controls, as shown by persistent p-S6 staining on western blot. Addition of rapamycin rescues the null cell ability to repress p-S6. **(B)** Schematic representation of *DEPDC5* with patient variants. Variants in red were shown to be loss-of-function mutants. **(C–J)** Representative plots of flow cytometry analysis performed on null cells transfected with variant constructs containing GFP in complete media and starved conditions, staining for p-S6. Mean percentage of cells in bottom right quadrant is indicated inside plots. **(K)** Box and whisker plot of quantification of transfected cells with low mTORC1 activity determined by flow cytometry analysis, indicating variant functional ability to repress mTORC1 in starved conditions. (**** = $p < .0001$, *** = $p < .001$, Two-way ANOVA with Dunnett's multiple comparisons tests, $n = 4–6$. **(L)** Western blot showing expression of *DEPDC5* variants and GFP marker in lysates of transfected *DEPDC5* null cells. (For interpretation of the references to colour in this figure legend, the reader is referred to the web version of this article.)

tested, loss-of-function was only observed in one missense *NPRL2* variant, three nonsense *NPRL3* variants, one indel *DEPDC5* variant and one nonsense *DEPDC5* variant. These results underline the importance of functional assessment of GATOR1 variants that are genetically implicated in disease causation.

2.3. A conditional model of a second-hit mutation of Depdc5 in the developing mouse brain has hyperactive mTORC1 and shows epileptic and FCD phenotypes

Having established defective mTORC1 regulation for some GATOR1 variants *in vitro*, we next investigated the role of mTORC1 in GATOR1-related epilepsy *in vivo*. To accurately model the 'second-hit' mechanism of disease, we first generated a *Depdc5* 'floxed' conditional mouse model using CRISPR/CAS9. The floxed allele includes loxP sites flanking exon 3 of *Depdc5* and the recombined product results in a frameshift (c.59_146del p.20Asp fs*25) (Supplemental Fig. 7A,B). We then generated $Depdc5^{flox/null}$ embryos using a previously generated constitutive null allele for *Depdc5* which has the same exon deleted (Hughes et al., 2017). For simplicity, $Depdc5^{flox/null}$ and $Depdc5^{flox/WT}$ mice will be referred to as flox/null and flox/WT hereafter. Finally, we used *in utero* electroporation to co-deliver plasmids encoding *Cre* recombinase (pCIG-Cre) and GFP (pCAG-GFP) to the brains of developing flox/null and flox/WT littermate embryos (14.5dpc). This generated GFP-positive null cell 'clones' within a heterozygous background thereby mimicking a second, somatic mutation in *Depdc5* during embryonic CNS development (Fig. 4A, Supplemental Fig. 7C). We confirmed *Cre* recombinase expression in GFP-positive neurons with an anti-CRE antibody and found very high levels of co-localisation (Fig. 4B). Additionally, to confirm recombination of the floxed allele in the presence of CRE, we amplified transcripts from GFP-sorted neurons from floxed embryos. Efficient generation of the null deletion allele was observed (Fig. 4C,D).

Given the elevated mTORC1 activity in GATOR1 null cell lines, we initially assessed the impact of clonal DEPDC5 deletion by assessing p-S6 levels. In adult mouse brains (P42) co-electroporated with *Cre*/GFP plasmids at 14.5dpc, we found that GFP-positive neurons in flox/null mice had a ~2-fold increase in p-S6 levels compared to flox/WT controls (Fig. 4E, F). Interestingly, we also observed elevated p-S6 expression in neighbouring GFP-negative neurons, indicating a possible cell non-autonomous effect. As mTORC1 controls cell growth, we also compared the soma size of GFP-positive flox/null and flox/WT neurons. We found that null neuron soma were on average 1.7 fold larger, and observed a range of sizes up to 3.5 fold larger than controls (Fig. 4E′, G, H). Some of these enlarged null neurons also exhibited an abnormal rounded morphology, similar to that seen in giant cells seen in tuberous sclerosis complex (TSC) patient tubers, or balloon cells seen in FCD type IIb (Fig. 4E′, H, I). Typically, balloon cells express immature markers such as Nestin, however, we did not see Nestin-positive neurons (data not shown) (Blümcke et al., 2011; Oh et al., 2008). We saw no difference in staining or localisation of SMI32 in flox/null tissue (data not shown). Rather, large dysmorphic neurons stained for NeuN, a mature neuronal marker, which may be more representative of FCD type IIa rather than type IIb (Fig. 4H) (Hu et al., 2018; Kabat and Król, 2012). The stellate morphology of *Depdc5*-null neurons indicated abnormal dendritic growth and arrangement. We therefore performed neuronal reconstruction analysis, which revealed that *Depdc5*-null neurons had a significant increase in the number of dendritic branch points, representing increased complexity and growth of flox/null dendrites compared to controls (Fig. 4I,J).

As cortical lamination is a feature of FCD type II, we measured the distribution of GFP-positive null neurons in layer II-III and layer IV. The majority of cells electroporated at 14.5dpc should migrate to layers II-III (Kwan et al., 2012; Ling et al., 2016; Ribierre et al., 2018). Indeed, we found over 80% of electroporated neurons in flox/WT cells at P42 were located in II/III, with the remaining in layer IV. However, in flox/null brains, only 39% of GFP-positive neurons were found in layers II/III while the remaining 61% neurons were in layer IV, indicating a migration defect across cortical layers II-IV (Fig. 5A–C). We did not observe ectopic neurons in any deeper cortical layers.

Given the epileptic phenotype of *DEPDC5* patients, we anticipated flox/null electroporated mice may be prone to seizures. As no overt spontaneous seizures were observed in flox/null or flox/WT mice during routine handling, we challenged the mice to a chemically induced seizure test using Pentylenetetrazol (PTZ). Administration of PTZ did not induce full generalised tonic-clonic (GTC) seizures in any flox/WT control mice within a 1-hour period, but was sufficient to induce GTC seizures in flox/null mice in 26 mins on average, indicating a significantly lowered seizure threshold (Fig. 5D).

Together, these data show that focal loss of *Depdc5* in mice causes hyperactivation of mTORC1 signalling and phenocopies GATOR1 deficiency in humans.

3. *In vivo* functional analysis of *DEPDC5* variants *F164del* and *Q542P*

Finally, we sought to investigate the function of two disease-associated *DEPDC5* variants in the context of the developing mammalian brain using the conditional 'second-hit' mouse model. We selected the relatively common F164del *DEPDC5* variant (confirmed *in vitro* to be loss-of-function) and Q542P (determined to be functional *in vitro*) to perform *in vivo* rescue experiments (Baldassari et al., 2018; Ricos et al., 2016). WT *DEPDC5,* F164del or Q542P expression constructs were co-electroporated with *Cre*/GFP plasmids at 14.5dpc (Fig. 4A). To confirm the successful electroporation and expression of the mutant, GFP-positive tissue was microdissected from P0 brains. RT-PCR amplification of cDNA transcript showed that the specific Flag-*DEPDC5* sequence was present only in the electroporated tissue for WT, F164del and Q542P constructs (Fig. 6A).

We first set out to determine if expression of F164del or Q542P in *Depdc5*-null neurons would rescue the mTORC1 hyperactivity in *Depdc5*-null neurons. In P15 mouse brains co-electroporated with WT DEPDC5 construct, GFP-neurons had p-S6 levels comparable to flox/WT controls, indicating a successful rescue of hyperactive mTORC1 of null neurons (Fig. 6B, C). Expression of Q542P also restored p-S6 levels to those of flox/WT controls consistent with our *in vitro* experiments. In contrast, p-S6 staining was ~2.6 fold higher in neurons electroporated with F164del compared with WT DEPDC5 rescue and flox/WT controls (Fig. 6B, C). While the p-S6 levels of F164del neurons were significantly higher than these controls, it is important to note that there remained a slight but significant difference between null neurons and F164del neurons, likely due to a low level of residual F164del function at high

Table 1
GATOR1 mutations found in patients, associated phenotypes and their functional status.

Gene	Mutation type	Nucleotide change	Protein change	Phenotypes	Penetrance	Function	Reference
Nprl2	Nonsense	c.100C > T	p. Arg34*	Nocturnal FLE	2 affected	Loss-of-function	Ricos et al., 2016
Nprl2	Missense	c.314T > C	p.Leu105Pro	Nocturnal FLE, FE, Nocturnal TCS, 1 unconfirmed seizures	5 affected, 1 unaffected	Loss-of-function	Ricos et al., 2016
Nprl2	Missense	c. 329C > G	p.Thr110Ser	TLE	1 affected, 1 unaffected	Yes	Ricos et al., 2016
Nprl2	Missense	c.640G > C	p.Asp214His	FLE	1 affected	Yes	Ricos et al., 2016
Nprl2	Nonsense	c. 883C > T	p.Arg295*	TLE	1 affected, 1unaffected	Yes	Ricos et al., 2016
Nprl3	Missense	c.275 G > A	p.Arg92Gln	FLE	1 affected, 1 unaffected	Yes	Ricos et al., 2016
Nprl3	Missense	c.745 G > A	p.Glu249Lys	Focal unspecified	1 affected	Yes	Ricos et al., 2016
Nprl3	Nonsense	c.835_836insT	p.Ser279Phe fs*52	Nocturnal FLE, Neonatal seizure, FB	4 affected, 2 unaffected	Loss-of-function	Ricos et al., 2016
Nprl3	Nonsense	c.954_955insCCCA	p.Trp319Pro fs*13	TLE	1 affected	Loss-of-function	Ricos et al., 2016
Nprl3	Nonsense	c.1376_1377insAC	p.Ser460Pro fs*20	TLE, Nocturnal TCS	2 affected	Loss-of-function	Ricos et al., 2016
Depdc5	Indel	c.488_490delTGT	p.Phe164del	FLE, Frontotemporal LE, TLE, occipital LE, unclassified seizures, Nocturnal FLE	35 affected, 15 unaffected	Loss-of-function	Dibbens et al., 2013
Depdc5	Missense	c.640C > G	p.His214Asp	Nocturnal FLE	1 affected, 1 unaffected	Yes	Ricos et al., 2016
Depdc5	Missense	c.842 A > T	p.Tyr281Phe	Epileptic spasms with FCD (encephalopathy), unclassified	3 affected	Yes	Carvill et al., 2015
Depdc5	Missense	c.1625 A > C	p.Gln542Pro	FS and occipital, temporo-occipital	2 affected	Yes	Ricos et al., 2016
Depdc5	Missense	c.3311C > T	p.Ser1104Leu	TLE	3 affected	Yes	Dibbens et al., 2013
Depdc5	Missense	c.3461C > T	p.Ser1154Phe	TLE, unclassified	2 affected, 1 unaffected	Yes	Ricos et al., 2016
Depdc5	Nonsense	c.4662_4663 del AG	p.Asp1556*	Epilepsy, Cortical dysplasia, lissencaphaly/pachygyria	1 affected	Loss-of-function	Cen et al., 2017

FLE – frontal lobe epilepsy.
FE- Focal epilepsy.
TLE – temporal lobe epilepsy.
TCS – tonic clonic seizures.
FB – Febrile seizures.

levels of expression.

We then measured soma size to determine whether this mTORC1 phenotype was rescued by Q542P or F164del expression. We compared soma sizes by layer and found that soma of layer II-III and layer IV *Depdc5*-null neurons were both larger than control neurons (Fig. 6D–F). We noticed that the fold change in size was not as drastic as those measured at P42 which suggests that null neurons may continue to grow larger over development and throughout adulthood, making the phenotype progressively more severe. The co-electroporation of WT DEPDC5 was sufficient to return the soma size to that of flox/WT control in both layers II-III and layer IV, confirming that the difference in soma size is a direct result of loss of *DEPDC5* function. *Depdc5*-null neurons expressing Q542P also were comparable to WT DEPDC5-expressing cells and flox/WT controls. On the other hand, *Depdc5*-null neurons expressing F164del were significantly larger than controls, showing that this null phenotype was not able to be rescued to normal size (Fig. 6D–F). Again, due to a predicted low level of function at high expression, the size of F164del-expressing level IV soma were significantly smaller than *Depdc5*-null neurons.

In summary, these data demonstrate that the recurrent F164del disease variant cannot fully rescue the clinically-relevant aberrant mTORC1 activity phenotypes that are generated *via* a *Depdc5* 'second-hit' *in vivo*. Conversely, variant Q542P, which was not functionally compromised *in vitro*, fully rescued the mTORC1 phenotype *in vivo*. Thus, compromised regulation mTORC1 signalling appears necessary and sufficient for manifestation of GATOR1 epilepsy/FCD *in vivo*.

4. Discussion

Mutations in the GATOR1 genes have been reported to be common causes of familial focal epilepsy, FCD type II and SUDEP (Baldassari et al., 2018). Despite previous GATOR1 loss-of-function studies implicating mTORC1 deregulation in the pathology, this long-standing hypothesis has yet to be confirmed for specific patient variants (Bar-Peled et al., 2013; Hu et al., 2018; Hughes et al., 2017; Ribierre et al., 2018). Understanding the functional activity of variants *in vitro* and *in vivo* will aid in diagnosis, predictions of disease outcome and targeted treatment for GATOR1 patients.

We first used GATOR1 null cell lines to perform *in vitro* functional screening analysis of 17 *NPRL2*, *NPRL3* and *DEPDC5* variants which were previously predicted to be pathogenic (Baldassari et al., 2018; Ricos et al., 2016). Our screening revealed that under starvation conditions, six variants: one missense *NPRL2* mutation (L105P), one in-frame *DEPDC5* indel mutation (F164del), one nonsense *DEPDC5* mutation (D1556*) and three nonsense *NPRL3* mutations (S279F fs*52, W319P fs*13, S460P fs*20) were unable to repress mTORC1 signalling, confirming that the mode of pathogenesis for these mutants is deregulation of the pathway.

Despite the incomplete (~65%) penetrance of *DEPDC5* F164del, this variant also has relatively strong genetic evidence of pathogenicity, being found in three large families with familial focal epilepsy with variable foci (FFEVF) (Dibbens et al., 2013). In concordance with our results, this variant has previously been confirmed to have a significant, although not complete, inability to regulate mTORC1 activity measured by phosphorylation of S6K in basal conditions (van Kranenburg et al., 2015). Although only identified as a *de novo* mutation in a single patient with epilepsy and pachygyria, the *DEPDC5* nonsense variant D1556* was also found to be loss-of-function (Cen et al., 2017). The only other two *DEPDC5* variants with proven loss-of-function are similar mutations (Q1523* and Q1536*) in the C-terminal domain (CTD) due to protein degradation, suggesting that the CTD has a role in DEPDC5 protein stability (Shen et al., 2018; van Kranenburg et al., 2015). All *NPRL3* variants found to be loss-of-function were nonsense mutations. All three had truncated the intermediary (INT) or CTD domains, which are predicted to be important for binding NPRL2 (Shen et al., 2018), and therefore may lead to loss-of-function through impaired GATOR1

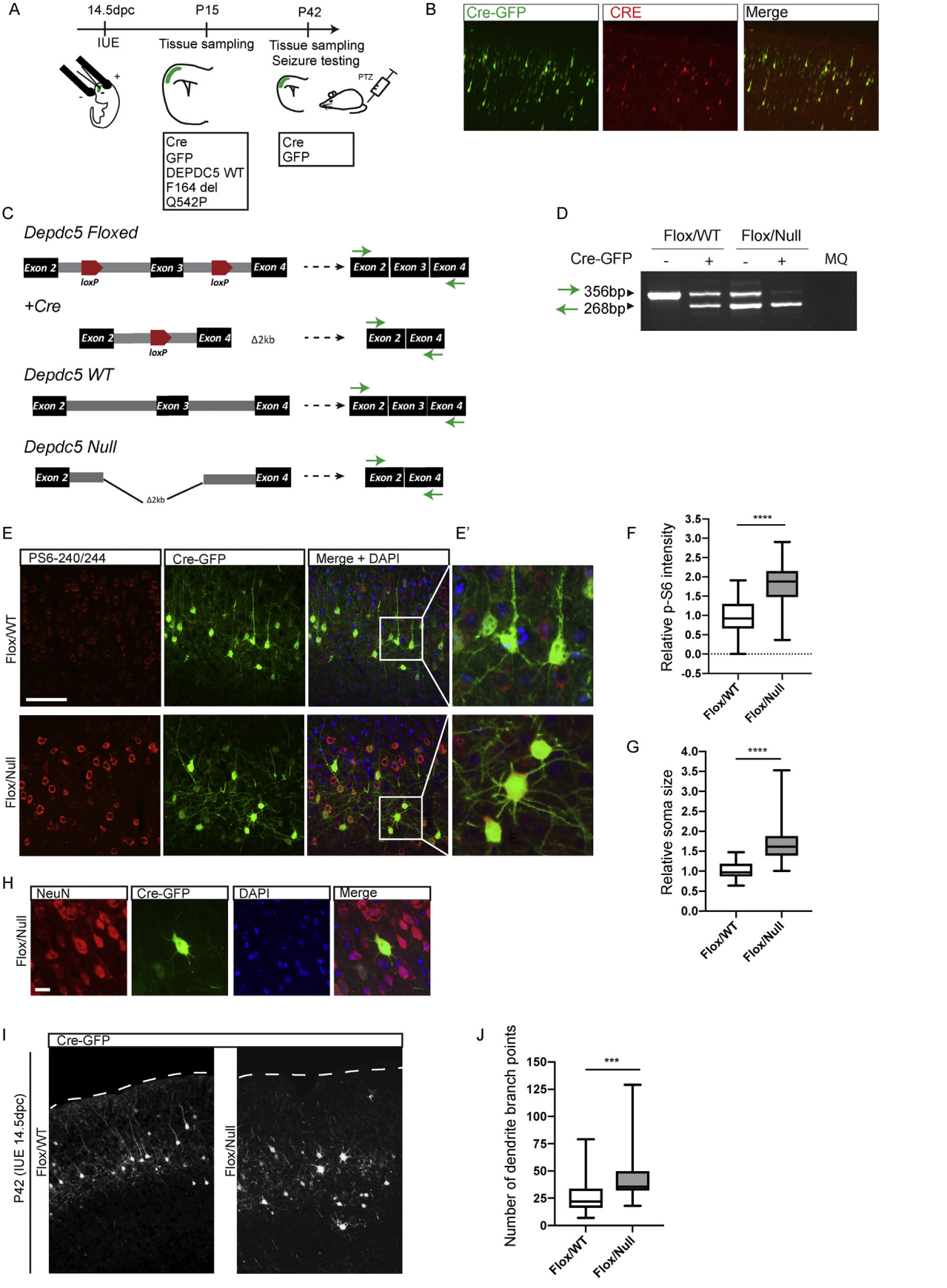

(caption on next page)

Fig. 4. Focal deletion of *Depdc5* in developing mouse brain using *in utero* electroporation results in large, dysmorphic neurons with hyperactive mTORC1 activity. (A) Schematic representation of *in vivo* DEPDC5 variant functional screening. **(B)** Immunostaining of electroporated 18.5dpc embryo brain using CRE antibody (red) shows co-expression with GFP-positive neurons. **(C)** Schematic representation of alleles- including floxed Depdc5 allele before and after the addition of Cre- and the resulting transcripts. Green arrows indicate primers used in PCRs in relation to cDNA for PCRs (left). **(D)** PCR using template cDNA from GFP-positive (Cre +) and GFP-negative (Cre -) brain cells from 18.5dpc brains electroporated at 14.5dpc showing the deletion of exon 3 in the transcripts (right). **(E)** Representative p-S6 immunostaining and GFP expression in P42 flox/null and flox/WT brains electroporated at 14.5dpc (scalebar = 100 μm). Boxes indicate region selected for higher magnification in (E'), showing a control neuron (top) and a large dysmorphic *Depdc5* null neuron (bottom, scale bar = 20 μm). Variability in soma size and morphology in null neurons is represented. (F) Box and whisker plot of p-S6 expression fold change in cortical GFP-positive neurons in flox/null mice (n = 9) normalised to flox/WT controls (n = 5) (**** = p < .0001, two-tailed unpaired *t*-test). (G) Box and whisker plot of fold change in soma size of cortical flox/null GFP-positive neurons normalised to flox/WT GFP-positive neurons (n = 11, n = 7 respectively, **** = p < .0001 two-tailed unpaired t-test). (H) Representative NeuN immunostaining showing expression in large *Depdc5* null neurons. (scale bar = 20 μm). (I) Representative images of increased dendritic branching of GFP-neurons in flox/null mice compared to flox/WT mice (scalebar = 100 μm). (J) Box and whisker plot of number of dendritic branch points obtained using neuronal filament tracing and reconstruction in flox/null brains (n = 4) and flox/WT brains (n = 4, *** = p < .001 two-tailed unpaired *t*-test). (For interpretation of the references to colour in this figure legend, the reader is referred to the web version of this article.)

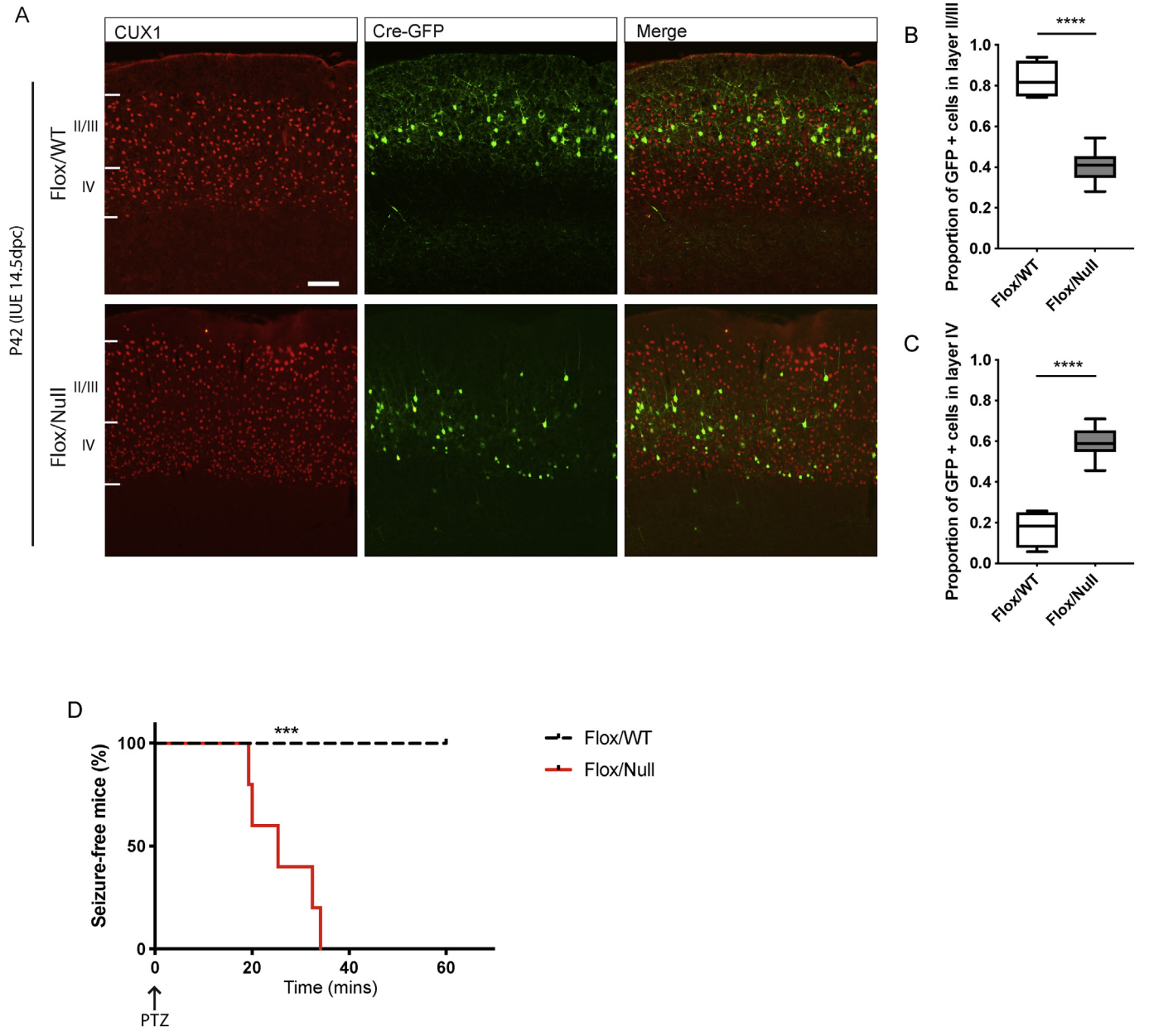

Fig. 5. *Depdc5* null neurons mice have migration defects and lower seizure thresholds. (A) Representative cortical images of P42 mice brains electroporated at 14.5pdc show the distribution of GFP-neurons in flox/null and flox/WT brains over cortical layers II-IV marked with CUX1 immunostaining (scale bar = 100 μM). **(B,C)** Box and whisker plot of the number of GFP-positive neurons in layer II/III **(B)** or layer IV **(C)** of P42 flox/null (n = 9) or flox/WT (n = 4) brains electroporated at 14.5dpc (**** = p < .0001, two-tailed unpaired *t*-tests). **(D)** Survival curve of PTZ seizure test shows increased seizure susceptibility in P42 *Depdc5* flox/null mice (n = 5) compared to flox/WT mice (n = 7) electroporated at 14.5dpc, (*** = p < .001 Mantel-Cox test).

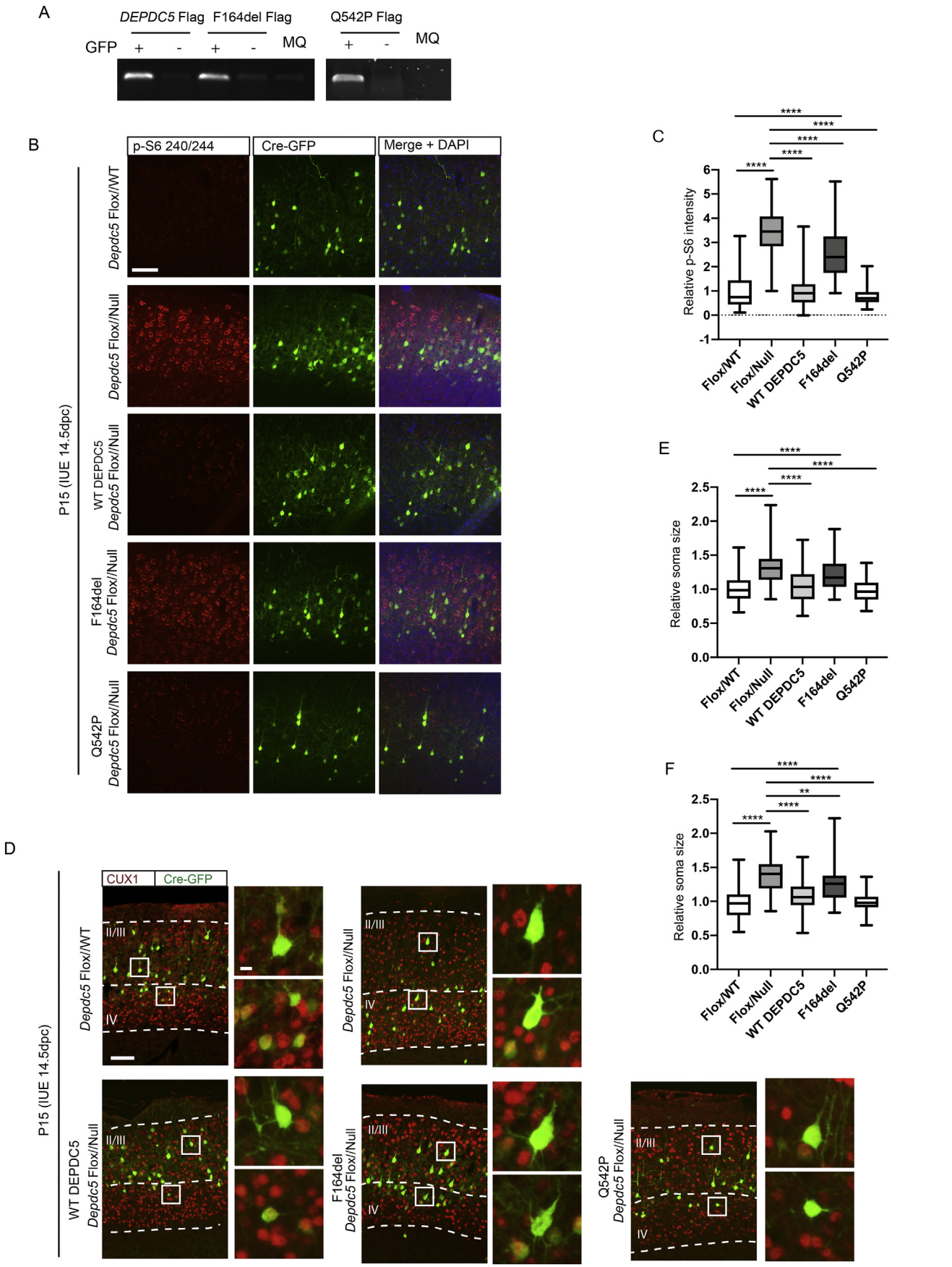

(caption on next page)

Fig. 6. *In vivo* functional testing of *DEPDC5* variants F164del and Q542P. (A) PCR of Flag sequence using cDNA template from GFP-positive (ipsilateral) and GFP-negative (contralateral) brain tissue from electroporated mouse brains (P0) showing the presence of the co-electroporated *Depdc5* constructs transcripts. **(B)** Representative p-S6 immunostaining of GFP-positive cortical neurons of *Depdc* flox/null P15 mice co-electroporated with WT *DEPDC5* WT, F164del or Q542P mutant constructs, and flox/null and flox/WT mice electroporated with Cre/GFP only (scalebar = 100 μm. **(C)** Box and whisker plot of the fold change in p-S6 expression shows P15 flox/null mice co-electroporated with WT *DEPDC5* (n = 6) and Q542P (n = 4) have p-S6 levels rescued to control levels (n = 10) while flox/null co-electroporated with F164del (n = 6) is comparable to flox/null mice electroporated with Cre-only (n = 6, **** = p < .0001 one-way ANOVA with Tukey's multiple comparisons tests). **(D)** Representative images of P15 cortices showing representative sizes of GFP-positive electroporated neuron soma (scalebar = 100 μm). CUX1 immunostaining (red) marks layers II-IV. One representative neuron for both layer II/II and layer IV is selected, for higher magnification (scale bar = 10 μm). **(E,F)** Box and whisker plots of fold change in soma size for P15 flox/null co-electroporated with WT, F164del or Q542P *Depdc5* constructs (n = 7, n = 9, n = 4 respectively) as well as flox/null and flox/WT Cre-only electroporated (n = 7, n = 9 respectively) control brains for layer II/III cortical GFP neurons, **(E)** and layer IV cortical GFP neurons **(F)** (**** = p < .0001, one-way ANOVA with Tukey's multiple comparisons tests). (For interpretation of the references to colour in this figure legend, the reader is referred to the web version of this article.)

complex formation. Only one *NPRL2* variant was functionally compromised (L105P). Although the genetic evidence for L105P disease causation is limited to a single three generation pedigree, this is nevertheless one of the most extensive pedigrees available for an *NPRL2* variant, which are typically reported in small nuclear families or in affected individuals harbouring *de novo* mutations. Furthermore, the recently solved structure of GATOR1 indicates that L105 is located within an α-helix which is proximal to an interaction interface between NPRL2 and DEPDC5. A proline substitution at this position may break or disrupt this α-helix and impair complex formation and/or affect the positioning of a nearby critical catalytic arginine residue (R78) (Richardson, 1981; Shen et al., 2019, 2018).

Interestingly, the majority of GATOR1 variants screened did not have significantly altered functional ability in the current *in vitro* assay despite previous predictions of their pathogenic nature (Carvill et al., 2015; Dibbens et al., 2013; Ricos et al., 2016). Indeed, of the nine GATOR1 missense mutations that we tested, only one was functionally compromised. This finding is consistent with a previous study on *DEPDC5* variants which found nine of 12 (75%) independent missense variants did not have significantly altered function (van Kranenburg et al., 2015). Furthermore, a recent prediction analysis has re-classified many GATOR1 variants of 'unknown significance' rather than 'likely pathogenic' (Baldassari et al., 2018; van Kranenburg et al., 2015). Notably however, *DEPDC5* H214D, which was classified as likely pathogenic, was found in our assay to function normally. Together, these findings highlight the importance of functional assessment for diagnosing variants as causative of disease, particularly for missense variants. Furthermore, the treatment of patients with these mutations using mTORC1 inhibitors such as rapamycin should be used with caution to avoid unnecessary side effects (Tran and Zupanc, 2015).

The GATOR1 null cell starvation rescue assay developed in this study should be useful in this regard with the following caveats. It is possible that variants with subtle functional defects or partial loss-of-function were not captured in our flow-based *in vitro* assay. Performing the screen in (disease relevant) neuronal cells may help identify tissue-specific effects of variants (or eliminate tissue specific compensatory mechanisms). *Ex vivo* electroporation and culture of organotypic brain slices may help identify subtle migration defects. Furthermore, the assay was conducted under complete nutrient depravation, and selectively evaluating the impact of specific amino acid depletion may increase the sensitivity of identifying pathological variants. Finally, variants were likely expressed above the endogenous levels, which may reduce the sensitivity of the assay. For example, *NPRL2* variant R34* (which showed slight, but not significantly altered function in our assay) may have deleterious physiological effects in endogenous conditions. The function retained in our assay may be due to the expression of the alternate isoform due to an alternate first exon (AFE) that falls after this mutation, which in our assay may be expressed above endogenous levels. It is also possible that some nonsense mutants found to be functional *in vitro* may be loss-of-function *in vivo* due to nonsense mediated decay (NMD).

To further our understanding of the pathological mechanism of *DEPDC5* disease variants, we developed a conditional mouse that modelled a somatic 'second-hit' *Depdc5* mutation during CNS development on a heterozygous background. This unique model exhibited pathogenic features redolent of epilepsy and FCD type II, including hyperactive mTORC1 signalling, large dysmorphic soma, increased dendritic branching, defective migration and lower seizure thresholds. These data support a 'second-hit' mechanism of disease and is consistent with the phenotypes recently described in other *Depdc5* rodent models (Hu et al., 2018; Ribierre et al., 2018; Yuskaitis et al., 2017). Our approach to modelling the human disease differs from previous studies in that the mice are germline heterozygotes before introduction of a second somatic mutation during development. Moreover, by employing the *Cre*/loxP system for the 'somatic hit', we can ensure that the somatic mutation causes complete loss-of-function. In contrast, other approaches utilise the CRISPR/CAS9 system on a WT background, where the mutational outcomes are variable and underlying global heterozygosity is not present (Hu et al., 2018; Ribierre et al., 2018). While the overall phenotype of published *Depdc5* focal deletion rodent models is relatively consistent, the sub-type classification of the FCD phenotype remains unresolved. Based on our inability to detect immature neuron marker Nestin or SMI32 in *Depdc5*-null neurons, our data favours a FCD type IIa classification, which is however not consistent with other models. While no *Depdc5*-null/Nestin-positive cells were detected in the rat model reported by Hu et al., this group did present aberrant cytoplasmic SMI32 expression, similar to findings from Yuskaitis et al. who showed disorganized SMI311 staining in the *Depdc5*-null mouse brain (Yuskaitis et al., 2017). Furthermore, balloon-like cells were reported in a conditional *Depdc5* mouse model by Ribierre et al. based on morphological and histopathological criteria, which concluded FCD type IIb. These FCD-like cells may become more apparent with age, as it may be the case that hyperactive mTORC1 activity has accumulative effects, and may explain the inconsistencies between models. With more patient samples and animal models, the finer classification of FCD related to GATOR1 genes should become clearer (Hu et al., 2018; Ribierre et al., 2018; Scerri et al., 2015; Sim et al., 2016; Weckhuysen et al., 2016).

We used this mouse model to further validate the functional status of two *DEPDC5* variants based on their contrasting activities in the *in vitro* null rescue experiments. *DEPDC5* variant Q542P, which has been recently classified as 'likely pathogenic' based on allele frequency and *in silico* prediction tools, was not functionally compromised in our *in vitro* assay (Baldassari et al., 2018). Consistent with the *in vitro* assay, expression of Q542P *in vivo* rescued mTORC1 hyperactivity and cytomegalic neurons in *Depdc5*-null cortices, indicating that this variant retains at least some function. Additional functional assessment of the Q542P variant should be performed to further investigate its potential pathogenesis. In contrast, the co-electroporation of functionally compromised F164del *DEPDC5* variant was unable to rescue null phenotypes to WT levels *in vivo* thereby providing independent confirmation of its pathogenicity. These *in vivo* data further validate our DEPDC5 *in vitro* functional assay and provide evidence that mTORC1 deregulation is necessary and sufficient for manifestation of *DEPDC5*-associated epilepsies. Testing seizure susceptibility and migration at later time points with whole-brain expression of *DEPDC5* variants would provide

further insight into variants that appear to have no functional impairment in our assays. Indeed, these variants require more investigation into their pathogenic ability, which may reveal the role of other undiscovered alternative pathogenic mechanisms. Given the functional interaction of DEPDC5 with NPRL2 and NPRL3, the validation of *DEPDC5* variant assay results *in vivo* indicates that the results of *NPRL2* and *NPRL3 in vitro* functional testing is likely reflective of their *in vivo* functional status. Thus, the *in vitro* assay and the *in vivo* mouse model rescue approach provide useful screening platforms for existing and emerging variants to contribute to a better understanding of functionally important regions and residues, allowing further refinement of classifications of disease causing variants.

While other models of hyperactive mTORC1 in the brain have also resulted in similar cortical malformation phenotypes, the specific mechanism by which mTORC1 hyperactivity causes epilepsy remain elusive (D'Gama et al., 2015; Goto et al., 2011; Park et al., 2018; Yuskaitis et al., 2017). The misplacement of neurons, abnormal size and morphology, and increased dendrite growth might lead to disrupted or inappropriate synaptic connections, which could manifest as seizures. However, previous investigations have shown that not all these architectural features may be necessary for causing seizures, suggesting that changes in other intrinsic electrogenic processes regulated by mTORC1 could lead to hyper-excitable neurons (Baulac, 2016; Hsieh et al., 2016; Magri et al., 2011). Therefore, while mTORC1 hyperactivity is an established molecular mechanism behind GATOR1 epilepsy and FCD, more investigation is required into which downstream effects lead to seizures. Additionally, further investigation into the possibility that mutations that affect mTORC1 regulation, whether in the same or different genes, may have an additive effect contributing to aberrant mTORC1 activity over a certain tolerable threshold and cause disease. Thus, it may be prudent to broaden the search for somatic mutations to include mTORC1 pathway genes that are not germline heterozygous (*e.g. NPRL2* or *NPRL3* in an affected *DEPDC5* germline heterozygous individual) and perform function assessment of candidate variants using the approach described herein (D'Gama et al., 2015; Park et al., 2018).

In conclusion, we employed *in vitro* and *in vivo* methods to functionally analyse GATOR1 variants and confirmed missense, in-frame deletion and nonsense variants in *NPRL2, NPRL3* and *DEPDC5* to be pathogenic. This data also provides the first *in vivo* evidence that *DEPDC5* variants have impaired functional ability to regulate mTORC1 signalling, and are therefore pathogenic. Additionally, our data supports that GATOR1 mutations may cause focal epilepsy and FCD through a second somatic hit mechanism. Finally, we demonstrate that many putative disease-causing variants retain function, highlighting the importance of functional screening in classification and diagnosis of disease variants.

5. Materials and methods

5.1. Patient mutations

NPRL2, *NPRL3* and *DEPDC5* variants were selected based on available literature with an emphasis on functional assessment of missense or in-frame mutations (Carvill et al., 2015; Cen et al., 2017; Dibbens et al., 2013; Ricos et al., 2016).

5.2. Cell culture

HEK293T cells were cultured in DMEM (GIBCO #12430062) with 10% FCS and 1% Glutamax incubated in 5% CO_2 at 37 °C. Starved conditions are in Earle's Balances Salt Solution (EBSS) for 1 h (GIBCO #14155063). Rapamycin 20 nM was added to EBSS for the rescue condition.

5.3. Generating GATOR1 null clones

Null lines for each of the GATOR1 genes were generated by co-transfecting cells with two CRISPR/CAS9 plasmids: pX458 (Addgene #48139) and pX459 (Addgene #62988), containing sgRNAs targeting regions flanking an exon for deletion leading to an early frameshift (Supplemental Fig. 1A). 24 h after transfection, cells underwent puromycin selection (2 μg/μL for 48 h). To select for PX458 plasmid transfection, only GFP-positive cells were grown. Cells were expanded to clonal cell lines and screened for exon deletion through PCR, or absence of protein by western blot (Supplemental Fig. 1B,C). For each of the three GATOR1 genes, two independent null cell lines were chosen for further experimentation in the mutation screening assay.

5.4. PCR based genotyping of null cell clones

DNA extraction from cells was performed with High Pure PCR Template purification Kit (Roche). Selection of null clone candidates was based on a PCR which amplified the region flanking the targeted exon and selected on size of predicted deletion. A secondary PCR was performed to confirm the exon deletion using primers within the exon sequence. PCR products were purified with QIAgen PCR Purification kit (CAT #28106) kit and Sanger sequenced performed by AGRF verified exon deletion.

5.5. Protein extraction and Western blots

Cell lysates were extracted using extraction buffer (150 mM NaCl, 1% NP-40, 0.5% deoxycholate, 0.1%SDS, 50 mM Tris-HCl pH 7.5) with protease inhibitor (Roche #4693159001) and phospho-stop tablets (Roche #4906845001), incubated at 4 °C for 30 min. Lysates were run on Invitrogen Bolt precast 4–12% polyacrylamide gels and transferred to PVDF membrane before blotting. Antibodies and their corresponding dilutions were: rabbit anti-NPRL3 1/500 (Sigma #HPA011741), mouse anti-NPRL2 1/1000 (Santa Cruz #sc-376986), mouse anti-Flag 1/1000 (Sigma #F3165), goat anti-GFP 1/5000 (Abcam ab5450).

5.6. Variant expression constructs

Flag-Nprl2 (#46333), Flag-Depdc5 pRK5 (#46340) and HA-Nprl3 (#46330) were purchased from Addgene. Variant constructs were generated with site-directed mutagenesis of these constructs using the QuikChange Lightning Site-Directed Mutagenesis kit (Agilent #210518). For *DEPDC5* variant S1104 L, exon 33 was cloned into Flag-Depdc5 pRK5 before mutagenesis.

5.7. Flow Cytometry

Flow cytometry analysis was performed 24 h after transfection and immediately after 1 h starvation. Cells were fixed with Cytofix™ (BD #554655), permeabilised in Phosflow™ Perm Buffer III (BD #558050) and stained for 1 h with primary antibody diluted in incubation buffer (PBS/0.5% bovine serum albumin) and 30 min with secondary antibody. Antibodies were: rabbit anti-phospho-S6 Ribosomal Protein (Ser240/244) (Cell Signalling, #5364, 1/100 [1 μg/μL]), Normal Rabbit IgG (Cell Signaling #3900, 1/1000 [1 μg/μL]), Alexa Fluor 647 (AbCam #ab150075, 1/2000). A minimum of 10,000 events were analysed for each sample with a BD Acuri™ C6. Analysis was performed with FlowJo software. Y-axis gating was based on P-S6 staining in complete media conditions, representing a threshold of high mTORC1 activity. X-axis gating was based on untransfected control cells.

5.8. Immunohistochemistry

Immediately after 1 h serum starvation, cells were fixed in 4% PFA/PBS for 15 min RT. Blocking in PBS/0.1% Triton X-100/10% horse

serum was performed for 30 min, followed by overnight incubation at 4 °C with primary antibody diluted in blocking solution. Cells were washed before a 2–4 h RT incubation with diluted secondary antibody. Slides were mounted in Prolong™ Gold Antifade with DAPI (Invitrogen #P36931).

For mouse brain immunofluorescence, P15 and P42 mice were euthanized with Lethabarb Euthanasia Injection and subject to cardiac perfusion with 4% PFA/PBS. Brains were dissected and fixed in 4% PFA overnight (a further 16 h) at 4 °C then cryoprotected in 30% sucrose overnight at 4 °C, and embedded in frozen OCT medium. 16 μm sections were cut from frozen tissue using Leica CM1900 cryostat. Tissue was blocked and stained as described above. Antibodies and their corresponding dilutions were: rabbit anti phospho-S6 Ribosomal Protein (Ser240/244) (Cell Signaling, #5364, 1:1000), mouse anti-NeuN 1/100 (Millipore, #MAB377), rabbit anti-Cre 1/400 (AbCam ab24607), mouse anti-Flag 1/1000 (Sigma #F3165), rabbit anti-Cux 1/400 (Santa Cruz #sc13024), chicken anti-GFP 1/1000 (Abcam ab13970).

All imaging was performed with a Nikon Eclipse Ti microscope and Nikon Digital Sight DS-Qi1 camera.

5.9. Animal housing and breeding

Experiments were performed on mice housed in IVC cages with a previously published null allele (Hughes et al., 2017) and a newly generated floxed allele generated with CRISPR/CAS9 (see below). These alleles were propagated in two separate colonies which were bred together using a flox/flox x null/WT cross to generate flox/null and flox/WT offspring for electroporation. *Depdc5* flox and null mice were generated and maintained on a C57BL/6J genetic background.

5.10. Generation of Depdc5 floxed mice

A pair of sgRNAs (5′-GATAGGGATACTGGTCTTCTAGG-3′, 5′-CTG ATCTCAAAAACTACTTCAGG-3′) were designed to flank exon 3 of *Depdc5* (mm9) and cloned into PX330. T7 PCR and IVT performed to generate sgRNA (Wang et al., 2013). Single stranded oligo donor sequences were designed containing loxP sequences (and restriction sites *EcoR1* and *Nhe1*) with 40 bp of homology either side, corresponding to either side of the targeted cut site.

C57BL/6J mouse zygotes were injected with both sgRNAs, oligo donors and spCas9 RNA in injection buffer and transferred to pseudopregnant females as previously described (Robertson et al., 2018). One founder mouse from these injections had a correctly targeted allele with both loxP sites inserted, which was confirmed first by separate PCRs and Sanger sequencing around the targeted regions. The loxP insertions were subsequently confirmed to be in *cis* after cloning of the PCR product spanning both sites into pGEMTeasy (#A1360) and sequencing from plasmid. The founder was crossed to C57BL/6J mice to generate F1 progeny carrying the floxed allele. F1 progeny were used to establish the flox colony.

5.11. Mouse genotyping

KAPA Express Extract Kit (Sigma KK7100) was used to purify genomic DNA from tail tips. For genotyping, the *Depdc5* floxed allele was identified based on by size after PCR amplifying around the region of loxP insertion. The following primers were used: *5' loxP site*: 5′-CATGCCTACCTACCTTGAATTTTT-3′, 5′-TCACAGGCACAAGCCAC TAC-3′; *3′ loxP site*: 5′- AGAGCTTCAGCCCAACTCTG-3′, 5′- CTGCACT CACATGCACAGG-3′ (annealing temperature 60°, Epicentre FailSafe 2× PreMix Buffer D). The *Depdc5* null allele was identified with a PCR using primers 5′-CATGCCTACCTACCTTGAATTTTT-3′, 5′-AACAGCCA GTGCTCTTACCAG-3′ (annealing temperature 62°, KAPA Taq Buffer A), which produces an amplicon around 500 bp indicating the 2 kb which includes exon 3. This PCR does not amplify the WT allele due to a short extension time. To identify the WT *Depdc5* allele, an internal PCR amplifying within the 2 kb region that is deleted in the null allele was used with primers 5′- GGCTGATCCGTGTGGAGTAT-3′, 5′- AGGGCCAC AACAGTAAATGG -3′ (annealing temperature 60°, Epicentre FailSafe 2× PreMix Buffer D).

6. *In utero* electroporation and plasmid preparation

In utero electroporation was performed on 14.5dpc embryos from pregnant time-mated females (from a flox/flox × null/WT cross) as previously described (Okada et al., 2007). Plasmids were purified with QIAgen *endo*-free Maxi kit (#12362) and concentrations were: pCAG-GFP plasmid, 1 μg/μL (Addgene #11150), pCIG-Cre, 1.5 μg/μL, Flag-DEPDC pRK5 3 μg/μL (Addgene #46340), Flag-Depdc5-F164del pRK5, 3 μg/μL, Flag-Depdc5-Q542P pRK5, 3 μg/μL. pCIG-Cre plasmid was a gift from Dr. Julian Heng. *DEPDC5* constructs were generated as described above and used equimolar to pCIG-Cre. pCAG-GFP plasmid was used at a lower concentration to decrease the likelihood of electroporation of only pCAG-GFP. 0.1% Fast Green was added to mix and 1-2 μL was injected into one lateral ventricle using a mouth pipette and pulled capillary needle (Harvard Apparatus #GC100TF-10).

7. *DEPDC5* transcript detection in vivo

GFP-positive 18.5dpc brain tissue was microdissected and trypsinised for 20 mins at 37 °C then aspirated with a Pasteur pipette to dissociate. BD FACSAria™ Fusion was used to sort the GFP-positive cells. RNA was extracted from sorted GFP-positive cells with TRIzol/chloroform protocol and purified with QIAgen RNeasy Mini Kit (ID #74104). cDNA was made from extracted RNA with Applied Biosciences High-Capacity cDNA RT Kit (#4368813). RT-PCR was performed on GFP positive and GFP negative cDNA to amplify the region surrounding the targeted exon to detect the deletion of the exon based on size using primers: 5′-GCAAGATGACTTCCCTGCTC-3′, 5′-CCACCAGGTCAAGAGTCACA-3′. RNA was extracted from P0 mice electroporated with DEPDC5 constructs to perform RT-PCR using primers amplifying the N-terminal FLAG and DEPDC5 sequence to confirm successful electroporation.

7.1. PTZ seizure test

85 mg/kg pentylenetetrazole (PTZ) was subcutaneously injected into P42 flox/WT ($n = 7$) and flox/null ($n = 5$) mice which were observed individually in clear cages for drug-induced seizure phenotypes culminating in tonic-clonic seizure. Time taken to generalised tonic-clonic (GTC) seizure was measured. Mice not reaching GTC seizure in 1 h were humanely euthanised.

7.2. Dendrite branching analysis

Confocal microscopy images of electroporated cortices were taken at 20× using (Olympus FV3000). Confocal images were analysed in IMARIS software (Bitplane) to perform filament tracing of GFP-neurons to predict/reconstruct dendritic structure. The z-series was reconstituted into a 3D image with IMARIS software and dendritic branch points were detected with Filament tracer software as previously described (Kaneko et al., 2011) and measured for (27–63) neurons per mouse (neurons present in field of view) for flox/null ($n = 4$) and flox/WT ($n = 4$). Fluorescence threshold parameters of dendrite detection was manually set above background.

7.3. Immunofluorescence analysis and statistical analysis

For *in vitro* functional assays, Two-Way Anovas with Dunnett's multiple comparisons tests against WT *NPRL2*, *NPRL3* or *DEPDC5* were performed ($n = 5$–7).

Immunofluorescence analysis was performed with Nikon NIS-

Elements software. For p-S6 240/244 analysis, mean fluorescence intensity was measured for 10 GFP-positive neurons randomly chosen on the DAPI channel, blinded to genotype (n = 7 flox/WT, n = 11 flox/null mice). Background non-stained levels of intensity was subtracted. Values were normalised to flox/WT control and Two tailed unpaired t-test was performed for P42 brains (flox/WT n = 5, flox/null n = 9). One-Way Anova with Tukey's multiple comparisons performed for P15 samples (flox/WT n = 9, flox/null n = 7, DEPDC WT n = 7, F164del n = 9, Q542P n = 4).

Soma size measurement was performed on 10–20 cells per mouse using freehand area tool on NIS-Elements software for flox/WT mice (n = 7) and flox/null (n = 11) P42 mice by drawing around the soma on the GFP channel. At P15, CUX1 and DAPI staining was used to distinguish layer II-III from layer IV based on cell density, and at least 10 GFP-positive soma from layer II-III or layer IV were measured per mouse for flox/WT mice (n = 9), flox/null (n = 7), F164del (n = 9) and Q542P (n = 4) were measured and analysed with one-way ANOVA with Tukey's multiple comparisons tests.

CUX1 and DAPI staining were used to define boundaries of layers II/III and IV of the cortex based on cell density and the location of GFP-positive neurons at P42 for n = 4 flox/WT mice and n = 6 flox/null were measured. The total number of cells per field of view at 10× magnification were counted and a proportion of cells in layers II/III was calculated. (Two-tailed unpaired t-test).

For dendritic branching analysis, 27–63 neurons per animal were subject to dendritic filament tracing, and number of dendritic branch points per neuron measured. Two-tailed unpaired t-test was used to compare number of dendritic branch points in flox/null (n = 4) and flox/WT (n = 4) mice.

PTZ survival curves for n = 7 flox/WT mice and n = 5 flox/null mice were compared with Mantel-Cox test.

All statistical analysis was performed on GraphPad Prism 7. Box and whisker plots show minimum and maximum range (whiskers) and are divided into two boxes and two whiskers, each representing 25% of the data. The middle bar represents median value.

7.4. Study approval

All animal work was conducted in accordance with Australian guidelines for the care and use of laboratory animals following approval by The University of Adelaide Animal Ethics committee and SAHMRI ethics committee (approval numbers S-2014-169, S-2015-200 and SAM254).

Author contributions

P.T, J.H and R.D conceived and designed the study. Mouse zygote injections were performed by S.P. A.N.G performed some *in utero* electroporation surgeries. L.R performed some immunostaining and assisted with figure preparation. All other experiments were performed by R.D. and analysed by R.D, A.N.G and P.T. Manuscript was prepared by R.D and P.T. All authors revised and approved the manuscript prior to submission.

Declaration of Competing Interest

The authors have declared that no conflict of interest exists.

Acknowledgements

This work was supported by funding from the Australian National Health and Medical Research Council. The authors would like to thank Dr. Julian Heng for the pCIG-Cre plasmid and technical advice with *in utero* electroporation work.

Appendix A. Supplementary data

Supplementary data to this article can be found online at https://doi.org/10.1016/j.nbd.2019.104640.

References

Bagnall, R.D., Crompton, D.E., Semsarian, C., 2017. Genetic basis of sudden unexpected death in epilepsy. Front. Neurol. 8. https://doi.org/10.3389/fneur.2017.00348.

Baldassari, S., Picard, F., Verbeek, N.E., van Kempen, M., Brilstra, E.H., Lesca, G., Conti, V., Guerrini, R., Bisulli, F., Licchetta, L., Pippucci, T., Tinuper, P., Hirsch, E., de Saint Martin, A., Chelly, J., Rudolf, G., Chipaux, M., Ferrand-Sorbets, S., Dorfmüller, G., Sisodiya, S., Balestrini, S., Schoeler, N., Hernandez-Hernandez, L., Krithika, S., Oegema, R., Hagebeuk, E., Gunning, B., Deckers, C., Berghuis, B., Wegner, I., Niks, E., Jansen, F.E., Braun, K., de Jong, D., Rubboli, G., Talvik, I., Sander, V., Uldall, P., Jacquemont, M.-L., Nava, C., Leguern, E., Julia, S., Gambardella, A., d'Orsi, G., Crichiutti, G., Faivre, L., Darmency, V., Benova, B., Krsek, P., Biraben, A., Lebre, A.-S., Jennesson, M., Sattar, S., Marchal, C., Nordli, D.R., Lindstrom, K., Striano, P., Lomax, L.B., Kiss, C., Bartolomei, F., Lepine, A.F., Schoonjans, A.-S., Stouffs, K., Jansen, A., Panagiotakaki, E., Ricard-Mousnier, B., Thevenon, J., de Bellescize, J., Catenoix, H., Dorn, T., Zenker, M., Müller-Schlüter, K., Brandt, C., Krey, I., Polster, T., Wolff, M., Balci, M., Rostasy, K., Achaz, G., Zacher, P., Becher, T., Cloppenborg, T., Yuskaitis, C.J., Weckhuysen, S., Poduri, A., Lemke, J.R., Møller, R.S., Baulac, S., 2018. The landscape of epilepsy-related GATOR1 variants. Genet. Med. doi:https://doi.org/10.1038/s41436-018-0060-2.

Bar-Peled, L., Chantranupong, L., Cherniack, A.D., Chen, W.W., Ottina, K.A., Grabiner, B.C., Spear, E.D., Carter, S.L., Meyerson, M., Sabatini, D.M., 2013. A tumor suppressor complex with GAP activity for the Rag GTPases that signal amino acid sufficiency to mTORC1. Science 340, 1100–1106. https://doi.org/10.1126/science.1232044.

Baulac, S., 2016. mTOR signaling pathway genes in focal epilepsies. Prog. Brain Res. 226, 61–79. https://doi.org/10.1016/bs.pbr.2016.04.013.

Baulac, S., Ishida, S., Marsan, E., Miquel, C., Biraben, A., Nguyen, D.K., Nordli, D., Cossette, P., Nguyen, S., Lambrecq, V., Vlaicu, M., Daniau, M., Bielle, F., Andermann, E., Andermann, F., Leguern, E., Chassoux, F., Picard, F., 2015. Familial focal epilepsy with focal cortical dysplasia due to DEPDC5 mutations. Ann. Neurol. 77, 675–683. https://doi.org/10.1002/ana.24368.

Blümcke, I., Thom, M., Aronica, E., Armstrong, D.D., Vinters, H.V., Palmini, A., Jacques, T.S., Avanzini, G., Barkovich, A.J., Battaglia, G., Becker, A., Cepeda, C., Cendes, F., Colombo, N., Crino, P., Cross, J.H., Delalande, O., Dubeau, F., Duncan, J., Guerrini, R., Kahane, P., Mathern, G., Najm, I., Özkara, Ç., Raybaud, C., Represa, A., Roper, S.N., Salamon, N., Schulze-Bonhage, A., Tassi, L., Vezzani, A., Spreafico, R., 2011. The clinico-pathological spectrum of focal cortical dysplasias: a consensus classification proposed by an ad hoc task force of the ILAE diagnostic methods commission. Epilepsia 52, 158–174. https://doi.org/10.1111/j.1528-1167.2010.02777.x.

Boillot, M., Baulac, S., 2016. Genetic models of focal epilepsies. J. Neurosci. Methods Methods Models Epilepsy Res. 260, 132–143. https://doi.org/10.1016/j.jneumeth.2015.06.003.

Carvill, G.L., Crompton, D.E., Regan, B.M., McMahon, J.M., Saykally, J., Zemel, M., Schneider, A.L., Dibbens, L., Howell, K.B., Mandelstam, S., Leventer, R.J., Harvey, A.S., Mullen, S.A., Berkovic, S.F., Sullivan, J., Scheffer, I.E., Mefford, H.C., 2015. Epileptic spasms are a feature of DEPDC5 mTORopathy. Neurol. Genet. 1, e17. https://doi.org/10.1212/NXG.0000000000000016.

Cen, Z., Guo, Y., Lou, Y., Jiang, B., Wang, J., Feng, J., 2017. De novo mutation in DEPDC5 associated with unilateral pachygyria and intractable epilepsy. Seizure 50, 1–3. https://doi.org/10.1016/j.seizure.2017.03.014.

D'Gama, A.M., Geng, Y., Couto, J.A., Martin, B., Boyle, E.A., LaCoursiere, C.M., Hossain, A., Hatem, N.E., Barry, B., Kwiatkowski, D.J., Vinters, H.V., Barkovich, A.J., Shendure, J., Mathern, G.W., Walsh, C.A., Poduri, A., 2015. mTOR pathway mutations cause hemimegalencephaly and focal cortical dysplasia. Ann. Neurol. 77, 720–725. https://doi.org/10.1002/ana.24357.

D'Gama, A.M., Woodworth, M.B., Hossain, A.A., Bizzotto, S., Hatem, N.E., LaCoursiere, C.M., Najm, I., Ying, Z., Yang, E., Barkovich, A.J., Kwiatkowski, D.J., Vinters, H.V., Madsen, J.R., Mathern, G.W., Blümcke, I., Poduri, A., Walsh, C.A., 2017. Somatic mutations activating the mTOR pathway in dorsal telencephalic progenitors cause a continuum of cortical dysplasias. Cell Rep. 21, 3754–3766. https://doi.org/10.1016/j.celrep.2017.11.106.

Dibbens, L.M., de Vries, B., Donatello, S., Heron, S.E., Hodgson, B.L., Chintawar, S., Crompton, D.E., Hughes, J.N., Bellows, S.T., Klein, K.M., Callenbach, P.M.C., Corbett, M.A., Gardner, A.E., Kivity, S., Iona, X., Regan, B.M., Weller, C.M., Crimmins, D., O'Brien, T.J., Guerrero-López, R., Mulley, J.C., Dubeau, F., Licchetta, L., Bisulli, F., Cossette, P., Thomas, P.Q., Gecz, J., Serratosa, J., Brouwer, O.F., Andermann, F., Andermann, E., van den Maagdenberg, A.M.J.M., Pandolfo, M., Berkovic, S.F., Scheffer, I.E., 2013. Mutations in DEPDC5 cause familial focal epilepsy with variable foci. Nat. Genet. 45, 546–551. https://doi.org/10.1038/ng.2599.

Goto, J., Talos, D.M., Klein, P., Qin, W., Chekaluk, Y.I., Anderl, S., Malinowska, I.A., Di Nardo, A., Bronson, R.T., Chan, J.A., Vinters, H.V., Kernie, S.G., Jensen, F.E., Sahin, M., Kwiatkowski, D.J., 2011. Regulable neural progenitor-specific Tsc1 loss yields giant cells with organellar dysfunction in a model of tuberous sclerosis complex. Proc. Natl. Acad. Sci. U. S. A. 108, E1070–E1079. https://doi.org/10.1073/pnas.1106454108.

Guo, D., Zeng, L., Brody, D.L., Wong, M., 2013. Rapamycin attenuates the development of posttraumatic epilepsy in a mouse model of traumatic brain injury. PLoS One 8, e64078. https://doi.org/10.1371/journal.pone.0064078.

Hesson, L.B., Cooper, W.N., Latif, F., 2007. Evaluation of the 3p21.3 tumour-suppressor gene cluster. Oncogene 26, 7283–7301. https://doi.org/10.1038/sj.onc.1210547.

Hsieh, L.S., Wen, J.H., Claycomb, K., Huang, Y., Harrsch, F.A., Naegele, J.R., Hyder, F., Buchanan, G.F., Bordey, A., 2016. Convulsive seizures from experimental focal cortical dysplasia occur independently of cell misplacement. Nat. Commun. 7, 11753. https://doi.org/10.1038/ncomms11753.

Hu, S., Knowlton, R.C., Watson, B.O., Glanowska, K.M., Murphy, G.G., Parent, J.M., Wang, Y., 2018. Somatic Depdc5 deletion recapitulates electroclinical features of human focal cortical dysplasia type IIA. Ann. Neurol. 84, 140–146. https://doi.org/10.1002/ana.25272.

Hughes, J., Dawson, R., Tea, M., McAninch, D., Piltz, S., Jackson, D., Stewart, L., Ricos, M.G., Dibbens, L.M., Harvey, N.L., Thomas, P., 2017. Knockout of the epilepsy gene Depdc5 in mice causes severe embryonic dysmorphology with hyperactivity of mTORC1 signalling. Sci. Rep. 7, 12618. https://doi.org/10.1038/s41598-017-12574-2.

Iffland, P.H., Baybis, M., Barnes, A.E., Leventer, R.J., Lockhart, P.J., Crino, P.B., 2018. DEPDC5 and NPRL3 modulate cell size, filopodial outgrowth, and localization of mTOR in neural progenitor cells and neurons. Neurobiol. Dis. 114, 184–193. https://doi.org/10.1016/j.nbd.2018.02.013.

Kabat, J., Król, P., 2012. Focal cortical dysplasia – review. Pol. J. Radiol. 77, 35–43.

Kaneko, M., Yamaguchi, K., Eiraku, M., Sato, M., Takata, N., Kiyohara, Y., Mishina, M., Hirase, H., Hashikawa, T., Kengaku, M., 2011. Remodeling of monoplanar Purkinje cell dendrites during cerebellar circuit formation. PLoS One 6, e20108. https://doi.org/10.1371/journal.pone.0020108.

van Kranenburg, M., Hoogeveen-Westerveld, M., Nellist, M., 2015. Preliminary functional assessment and classification of DEPDC5 variants associated with focal epilepsy. Hum. Mutat. 36, 200–209. https://doi.org/10.1002/humu.22723.

Kwan, K.Y., Šestan, N., Anton, E.S., 2012. Transcriptional co-regulation of neuronal migration and laminar identity in the neocortex. Development 139, 1535–1546. https://doi.org/10.1242/dev.069963.

Ling, W., Endo, T., Kubo, K.-I., Nakajima, K., Kakeyama, M., Tohyama, C., 2016. In utero bisphenol a exposure induces abnormal neuronal migration in the cerebral cortex of mice. Front. Endocrinol. (Lausanne) 7, 7. https://doi.org/10.3389/fendo.2016.00007.

Lipton, J.O., Sahin, M., 2014. The neurology of mTOR. Neuron 84, 275–291. https://doi.org/10.1016/j.neuron.2014.09.034.

Magri, L., Cambiaghi, M., Cominelli, M., Alfaro-Cervello, C., Cursi, M., Pala, M., Bulfone, A., Garcìa-Verdugo, J.M., Leocani, L., Minicucci, F., Poliani, P.L., Galli, R., 2011. Sustained activation of mTOR pathway in embryonic neural stem cells leads to development of tuberous sclerosis complex-associated lesions. Cell Stem Cell 9, 447–462. https://doi.org/10.1016/j.stem.2011.09.008.

Meng, X.-F., Yu, J.-T., Song, J.-H., Chi, S., Tan, L., 2013. Role of the mTOR signaling pathway in epilepsy. J. Neurol. Sci. 332, 4–15. https://doi.org/10.1016/j.jns.2013.05.029.

Møller, R.S., Weckhuysen, S., Chipaux, M., Marsan, E., Taly, V., Bebin, E.M., Hiatt, S.M., Prokop, J.W., Bowling, K.M., Mei, D., Conti, V., de la Grange, P., Ferrand-Sorbets, S., Dorfmüller, G., Lambrecq, V., Larsen, L.H.G., Leguern, E., Guerrini, R., Rubboli, G., Cooper, G.M., Baulac, S., 2016. Germline and somatic mutations in the MTOR gene in focal cortical dysplasia and epilepsy. Neurol. Genet. 2. https://doi.org/10.1212/NXG.0000000000000118.

Nascimento, F.A., Borlot, F., Cossette, P., Minassian, B.A., Andrade, D.M., 2015. Two definite cases of sudden unexpected death in epilepsy in a family with a DEPDC5 mutation. Neurol. Genet. 1, e28. https://doi.org/10.1212/NXG.0000000000000028.

Oh, H.-S., Lee, M.-C., Kim, H.-S., Lee, J.-S., Lee, J.-H., Kim, M.-K., Woo, Y.-J., Kim, J.-H., Kim, H.-I., Kim, S.-U., 2008. Pathophysiologic characteristics of balloon cells in cortical dysplasia. Childs Nerv. Syst. 24, 175–183. https://doi.org/10.1007/s00381-007-0453-z.

Okada, T., Keino-Masu, K., Masu, M., 2007. Migration and nucleogenesis of mouse precerebellar neurons visualized by in utero electroporation of a green fluorescent protein gene. Neurosci. Res. 57, 40–49. https://doi.org/10.1016/j.neures.2006.09.010.

Park, S.M., Lim, J.S., Ramakrishina, S., Kim, S.H., Kim, W.K., Lee, J., Kang, H.-C., Reiter, J.F., Kim, D.S., Kim, H.H., Lee, J.H., 2018. Brain somatic mutations in MTOR disrupt neuronal ciliogenesis, leading to focal cortical dyslamination. Neuron 99, 83–97.e7. https://doi.org/10.1016/j.neuron.2018.05.039.

Ribierre, T., Deleuze, C., Bacq, A., Baldassari, S., Marsan, E., Chipaux, M., Muraca, G., Roussel, D., Navarro, V., Leguern, E., Miles, R., Baulac, S., 2018. Second-hit mosaic mutation in mTORC1 repressor DEPDC5 causes focal cortical dysplasia-associated epilepsy. J. Clin. Invest. 128, 2452–2458. https://doi.org/10.1172/JCI99384.

Richardson, J.S., 1981. The anatomy and taxonomy of protein structure. In: Anfinsen, C.B., Edsall, J.T., Richards, F.M. (Eds.), Advances in Protein Chemistry. Academic Press, pp. 167–339. https://doi.org/10.1016/S0065-3233(08)60520-3.

Ricos, M.G., Hodgson, B.L., Pippucci, T., Saidin, A., Ong, Y.S., Heron, S.E., Licchetta, L., Bisulli, F., Bayly, M.A., Hughes, J., Baldassari, S., Palombo, F., Epilepsy Electroclinical Study Group, Santucci, M., Meletti, S., Berkovic, S.F., Rubboli, G., Thomas, P.Q., Scheffer, I.E., Tinuper, P., Geoghegan, J., Schreiber, A.W., Dibbens, L.M., 2016. Mutations in the mammalian target of rapamycin pathway regulators NPRL2 and NPRL3 cause focal epilepsy. Ann. Neurol. 79, 120–131. https://doi.org/10.1002/ana.24547.

Robertson, L., Pederick, D., Piltz, S., White, M., Nieto, A., Ahladas, M., Adikusuma, F., Thomas, P.Q., 2018. Expanding the RNA-guided endonuclease toolkit for mouse genome editing. CRISPR J. 1, 431–439. https://doi.org/10.1089/crispr.2018.0050.

Scerri, T., Riseley, J.R., Gillies, G., Pope, K., Burgess, R., Mandelstam, S.A., Dibbens, L., Chow, C.W., Maixner, W., Harvey, A.S., Jackson, G.D., Amor, D.J., Delatycki, M.B., Crino, P.B., Berkovic, S.F., Scheffer, I.E., Bahlo, M., Lockhart, P.J., Leventer, R.J., 2015. Familial cortical dysplasia type IIA caused by a germline mutation in DEPDC5. Ann. Clin. Transl. Neurol. 2, 575–580. https://doi.org/10.1002/acn3.191.

Shen, K., Huang, R.K., Brignole, E.J., Condon, K.J., Valenstein, M.L., Chantranupong, L., Bomaliyamu, A., Choe, A., Hong, C., Yu, Z., Sabatini, D.M., 2018. Architecture of the human GATOR1 and GATOR1–Rag GTPases complexes. Nature. https://doi.org/10.1038/nature26158.

Shen, K., Valenstein, M.L., Gu, X., Sabatini, D.M., 2019. Arg78 of Nprl2 catalyzes GATOR1-stimulated GTP hydrolysis by the Rag GTPases. J. Biol. Chem. https://doi.org/10.1074/jbc.AC119.007382.

Sim, J.C., Scerri, T., Fanjul-Fernández, M., Riseley, J.R., Gillies, G., Pope, K., van Roozendaal, H., Heng, J.I., Mandelstam, S.A., McGillivray, G., MacGregor, D., Kannan, L., Maixner, W., Harvey, A.S., Amor, D.J., Delatycki, M.B., Crino, P.B., Bahlo, M., Lockhart, P.J., Leventer, R.J., 2016. Familial cortical dysplasia caused by mutation in the mammalian target of rapamycin regulator NPRL3. Ann. Neurol. 79, 132–137. https://doi.org/10.1002/ana.24502.

Thomas, R.H., Berkovic, S.F., 2014. The hidden genetics of epilepsy-a clinically important new paradigm. Nat. Rev. Neurol. 10, 283–292. https://doi.org/10.1038/nrneurol.2014.62.

Tran, L.H., Zupanc, M.L., 2015. Long-term Everolimus treatment in individuals with tuberous sclerosis complex: a review of the current literature. Pediatr. Neurol. 53, 23–30. https://doi.org/10.1016/j.pediatrneurol.2014.10.024.

Wang, H., Yang, H., Shivalila, C.S., Dawlaty, M.M., Cheng, A.W., Zhang, F., Jaenisch, R., 2013. One-step generation of mice carrying mutations in multiple genes by CRISPR/Cas-mediated genome engineering. Cell 153, 910–918. https://doi.org/10.1016/j.cell.2013.04.025.

Weckhuysen, S., Marsan, E., Lambrecq, V., Marchal, C., Morin-Brureau, M., An-Gourfinkel, I., Baulac, M., Fohlen, M., Kallay Zetchi, C., Seeck, M., de la Grange, P., Dermaut, B., Meurs, A., Thomas, P., Chassoux, F., Leguern, E., Picard, F., Baulac, S., 2016. Involvement of GATOR complex genes in familial focal epilepsies and focal cortical dysplasia. Epilepsia 57, 994–1003. https://doi.org/10.1111/epi.13391.

Yuskaitis, C.J., Jones, B.M., Wolfson, R.L., Super, C.E., Dhamne, S.C., Rotenberg, A., Sabatini, D.M., Sahin, M., Poduri, A., 2017. A mouse model of DEPDC5-related epilepsy: neuronal loss of Depdc5 causes dysplastic and ectopic neurons, increased mTOR signaling, and seizure susceptibility. Neurobiol. Dis. 111, 91–101. https://doi.org/10.1016/j.nbd.2017.12.010.